Hindawi
Advances in Civil Engineering
Volume 2023, Article ID 6192001, 13 pages
https://doi.org/10.1155/2023/6192001

Research Article

Semi-automated Generation of Geometric Digital Twin for Bridge Based on Terrestrial Laser Scanning Data

Kaixin Hu,[1] **Daguang Han**,[2] **Guocheng Qin**,[3] **Yin Zhou**,[4] **Long Chen**,[5] **Chunli Ying**,[1] **Tong Guo**,[2] **and Yanhui Liu**[6]

[1]*Chongqing Smart City and Sustainable Development Academy, Chongqing 401135, China*
[2]*School of Civil Engineering, Southeast University, Nanjing 211100, China*
[3]*Cadastral Investigation Institute, Chongqing Institute of Surveying and Monitoring for Planning and Natural Resources, Chongqing 401147, China*
[4]*Department of Civil Engineering, Chongqing Jiaotong University, Chongqing 400074, China*
[5]*College of Architecture and Civil Engineering, Loughborough University, Loughborough LE113TU, UK*
[6]*School of Civil Engineering, Southwest Jiaotong University, Chengdu 610000, China*

Correspondence should be addressed to Daguang Han; daguangh@oslomet.no

Received 28 December 2021; Revised 17 August 2022; Accepted 22 September 2022; Published 7 March 2023

Academic Editor: Jiarui Lin

Digital twins (DTs) have a great potential for bridge operation and maintenance. Geometric digital twins (gDTs) are the key component of DTs. At present, a growing number of researchers are using high-precision 3D laser point clouds to generate gDTs. However, for large bridges, such as arch, cable-stayed, and suspension bridges, comprehensive point-cloud collection stations are difficult to set up due to their large span, narrow site, and limited field of vision. Consequently, the complete point clouds of these bridges cannot be easily obtained. Thus, knowing how to process absence point clouds and generate gDTs is an urgent problem. This study proposes a semiautomatic method of extracting geometric information of a bridge's components in the absence of point clouds. First, an algorithm based on the combination of the iterative polynomial fitting curve and sliding window is developed to extract the arch ring accurately. Second, an improved random sample consensus (RANSAC) algorithm based on distribution density is adopted to extract the cross sections of the arch bridge components, except the arch ring. For cross sections that lack point clouds, a translation strategy is used to supplement the unknown line segment. Finally, for the T-beam, a model alignment method is proposed to best match the characteristic intersections extracted by the improved RANSAC algorithm and the points corresponding to the design model. The quality of the generated models is gauged using a point cloud deviation chromatogram. In addition, the stressed component piers are compared with its design parameters to verify the accuracy of the proposed method. Results show that our method can efficiently and accurately extract geometric information and generate gDT for the bridge.

1. Introduction

Bridge safety has become a common research topic because bridges are an important part of highway infrastructure and are exposed to many dangers during their lifecycle [1]. After a bridge is built and used, knowing how to manage and maintain them is a long and costly task. Previous studies have proven that operation and maintenance costs account for half of the total costs of bridges in their lifecycle [2].

An essential problem in the operation and maintenance of bridges is efficient data storage. Nevertheless, the emergence of digital twins (DTs) has provided an effective approach to address this problem. DTs are digital copies of real-world assets [3], consisting of a 3D geometric digital twin (gDT) and semantic, material, and mechanical information. Among them, gDT is the key component. In the bridge design stage, engineers build 3D models of a bridge design according to 2D drawings. However, differences exist between the designed 3D model and gDT due to deviations

in construction [4]. To obtain gDTs, the appearance and process of a bridge and the corresponding data should be tested upon bridge completion and during its operation [5]. Building information modeling (BIM) is an effective approach of realizing parametric modeling, and it is particularly suitable for generating gDTs.

Terrestrial laser scanning (TLS) is an advanced technology used to obtain building information quickly. TLS has surpassed some traditional measurement methods [6]. Furthermore, TLS can accurately and comprehensively obtain the surface points (i.e., point clouds) of a detected object. However, TLS is mainly used to obtain and process the information of simple components, such as buildings, pipelines, and simple supported beams [7–10]. Most of these objects have simple or single components; thus, some methods are unsuitable for directly analyzing bridge components. In recent years, relevant research on bridge measurement and modeling using TLS has been conducted. Given its simple structure and wide distribution, simply supported beam bridges have become a main research object of bridge point clouds. Lu and Brilakis [11] delivered a slicing-based object fitting method that can generate the gDT of an existing reinforced concrete bridge from four types of labeled point clusters. An average modeling distance of 7.05 cm of gDT was obtained. Qin et al. [12] proposed an automatic method of reconstructing parameterized BIM by using point clouds to target simply supported beam bridges, and the accuracy was within 2 cm. For arch bridges with a complex structure, point clouds have more advantages than traditional total station measurement. Yang et al. [13] used an iterative polynomial algorithm to fit the arch structure alignment in the laboratory and obtained data of thirteen epochs. Results showed the reliability of 3D laser scanning and its advantages over traditional methods. Riveiro et al. [14] presented a new method for fully automated point cloud segmentation of masonry arch bridges. The method efficiently created segmented, spatially related, and organized point clouds, each containing relevant geometric data for a particular component (pier, arch, spandrel wall, etc.) of the structure. Occlusions and areas of low point density can cause elements to be missed or classified as noise. To address the problems that most existing methods for creating as-built BIMs from laser scanning data involve plenty of manual work, Yang et al. [15] conducted semi-automated generation of parametric BIM based on TLS data for complex steel structures. The authors believed that future research is needed to extend the developed technology to other common types of structural components, such as L-shaped components, T-shaped components, and other components formed by combining basic primitives.

TLS has great potential in the research of long-span arch bridges. First, with the arch ring as the main force-bearing object of arch bridges, the existing methods are not accurate enough for its local details. Furthermore, for large bridges, such as arch, cable-stayed, and suspension bridges, comprehensive data collection stations are difficult to set up because of their large span, narrow site, and limited field of vision. Therefore, complete point clouds are also difficult to obtain. Knowing how to process data and generate gDT in the absence point clouds is an urgent problem. Thus, this study proposes a method of processing the absence point clouds and gDT generation. The main contributions of this method are as follows: (1) an algorithm based on the combination of the iterative polynomial fitting curve and the sliding window is developed to extract the arch ring accurately. (2) An improved random sample consensus (RANSAC) algorithm based on distribution density is adopted to extract the cross sections of arch bridge components except the arch ring. (3) Finally, for the T-beam, a model alignment method is proposed to best match the characteristic intersections extracted by the improved RANSAC algorithm and the points corresponding to the design model. The quality of the generated models is gauged using a point cloud deviation chromatogram. In addition, the stressed component piers are compared with its design parameters to verify the accuracy of the proposed method. Three algorithms are used to extract the geometric information of the arch bridge components, and the arch bridge gDT is parameterized using BIM software.

The remainder of this paper is organized as follows: Section 2 provides the research background with respect to the three aspects of bridge gDT generation: shape representation, geometric information extraction, and bridge gDT generation. The developed approach to extract geometry information from laser scanning data and generate gDT is described in Section 3. Section 4 presents illustrative examples to validate the proposed method and discusses the experimental results. Section 5 provides a summary and the conclusion of this study.

2. Related Work Background

The two kinds of point-cloud reverse-generation models are the 3D grid models [16] and geometric structures [17], and they are defined in accordance with curve shapes, vertical elevations, and cross sections. The former reconstruction method is simple, but it cannot be used with gDT to collect other information. The latter is an essential approach to gDT, and it generates data for logical objects that can be used to model the visualization and modification of these objects. In general, gDT generation for arch bridges consists of the following steps: (1) shape representation, (2) geometric information extraction, and (3) bridge gDT generation.

2.1. Shape Representation Method. No universal solution can describe 3D objects, and different representations have their own advantages and disadvantages. The choice of a shape representation method depends on the preferred modeling technology and the characteristics of the target object. The most commonly used shape representation methods can be divided into four categories: implicit representation, boundary representation, constructed solid geometry, and swept solid representation (SSR). Implicit representation requires mathematical formulas to represent 3D shapes, and it has the advantage of accurately describing the 3D shape of the object, i.e., whether it is a plane [18], a sphere, a ring [19], and so on. However, implicit representation can hardly

represent edges and vertices. Boundary representation provides information about each vertex, edge, and cycle, and it describes shapes by using their limits, thus overcoming the weakness of implicit representation. However, the results of boundary representation may be highly complicated due to the required high-resolution detail level [20], which is detrimental to operations and maintenance. Constructive solid geometry is a set of basic entity primitives that follow a certain "logic." A basic body can be in the form of a cuboid, cylinder, sphere, cone, and so on. The random sampling method of Schnabel et al. [19] can be used to model objects comprising five basic shapes: plane, sphere, cylinder, cone, and torus. Nguyen et al. [9] proposed the fitting of a segmented cylinder on the basis of normal region growth to segment and identify pipeline components. However, the shapes of bridge components are generally complex. The method of constructed solid geometry can be described as an idealized or simplified topology design, but bridge components, such as arch ring, cable, T-beam, are difficult to describe accurately. As a representation model, SSR creates a 3D shape by sweeping a 2D cross section along a specific path. Arch ring alignment, pier verticality, and cable sag are important parameters of bridges, and they can be described by a 3D path. In addition, most bridge components have a uniform section; thus, the cross section is fixed. Therefore, SSR is a suitable shape representation method to describe bridges [11, 12, 15].

2.2. Geometric Information Extraction. SSR includes two aspects: 2D cross section and 3D sweep path. Many studies have attempted to obtain the 2D cross section of point clouds. Ramamurthy et al. [21] extracted geometric features, such as line segments related to cross sections, from point clouds that contain noise and rough surfaces. Moreira et al. [22] used the concave packet algorithm to extract the concave hulls of a local XY plane of a slice. Laefer and Hong [23] proposed a kernel density estimation method to reconstruct the point cloud of standard steel beams in a BIM-compatible format. Zhou et al. [24] developed a parameter extraction method based on grid points to extract quickly and effectively bolt hole features. As for obtaining a 3D sweep path of point clouds, the line shape of the curve component with respect to a straight line is difficult to extract. Bauer and Polthier [25] proposed an automatic method of parametric reconstruction of a curved surface by using unorganized point sets. They applied the principle of using the moving least square method to calculate the spine curve of the pipe surface and approximate the polygon curve via the continuous arc spline. To obtain the deformation of each stage of an arch ring accurately, Yang et al. [13] defined the best-fitting surface and changed the usual order to move the polynomial surface closer to the actual point cloud.

For large bridges, such as arch, cable-stayed, and suspension bridges, comprehensive point-cloud collection stations are difficult to set up because of their large span, narrow site, and limited field of vision. Consequently, the complete point clouds of these bridges are also difficult to obtain. Knowing how to process absence point clouds and generate gDT is an urgent problem. Yang et al. [15] extracted data from 39 pillars of a bridge for a large-scale bridge-like steel structure and completed an as-built BIM. In achieving a complete model, the modeling parameters of the two missing struts in their work and the corresponding connection plates were manually generated. The arch ring is the main bearing component of an arch bridge, and thus, ensuring its high-precision alignment is important. Knowing how to process absence point clouds is another urgent problem. Thus, an improved RANSAC algorithm based on distribution density is adopted in this study to extract the sections of arch bridge components except the arch ring. For sections that lack point clouds, the translation strategy is used to supplement the unknown line segment. For the T-beam, a model-matching algorithm is used to best align the design model and gDT.

2.3. Bridge gDT Generation. In contrast to the component model generation of bridges, that of buildings is relatively simple. Jung et al. [26] built the inner and outer walls of buildings through point cloud segmentation and feature recognition. The object of their study only included a single type of a component. Danielle et al. [27] suggested the use of a data-processing algorithm as provided by a point cloud library to create walls and floors. For the common existence of simple and complex shapes, Barazzetti et al. [28] proposed a parametric BIM generation method that can preliminarily separate two aspects. For simple shape modeling, commercial BIM software is used. For complex shape modeling, nonuniform rational basis splines are utilized. Commercial BIM software provides powerful tools for modelers, and it is the platform of choice for most modelers. Quattrini et al. [29] used Autodesk Recap and Revit to create 3D models directly from point cloud data and subsequently modeled them using parameterized elements in Revit (i.e., built-in family library and custom family). However, current experience suggests that no software can perform all geometric modeling [30].

Most software platforms support only a few standard components, such as wall and pipe modeling [31]. In addition, information may be lost due to manual modeling operations [32]. Thus, modeling efficiency is difficult to ensure [33]. In this study, the CATIA platform, which is known for its powerful parameterization ability, is adopted to generate arch bridge gDT.

3. Methods

3.1. Overview. This section describes the semi-automated generation of gDT for arch bridge based on TLS data. For large bridges, such as arch, cable-stayed, and suspension bridges, comprehensive point cloud collection stations are difficult to set up because of their large span, narrow site, and limited field of vision. Therefore, the object of this study is the absence point cloud.

Figure 1 shows an overview of our method that includes three steps: (1) data segmentation, (2) extraction of the bridge components' geometric information, and (3)

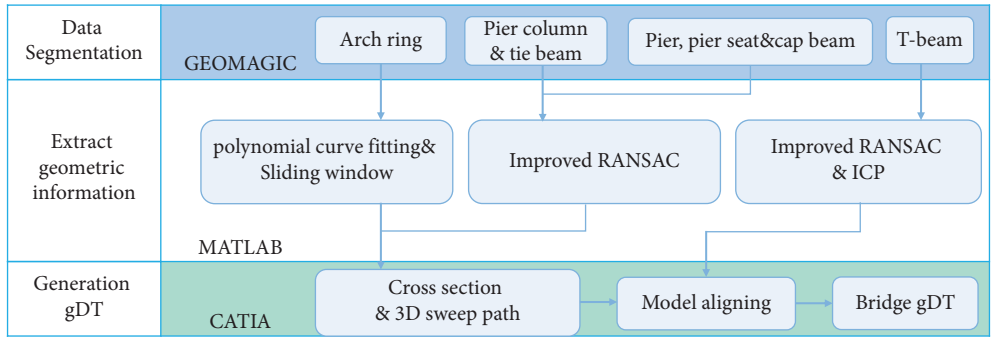

Figure 1: Overview of the proposed method for arch bridge gDT generation.

parametric bridge gDT generation. Section 3.2 introduces that the point cloud processing software Geomagic is used to separate different components of the arch bridge and classify them into different categories. Section 3.3 discusses the algorithms that have been developed and implemented in MATLAB for various components to extract the bridge components' geometric information. Among them, each object class has its own workflow. Section 3.4 presents the process of how to generate the parametric bridge gDT in CATIA. In this study, all solutions of bridge component generation are in SSR.

The assumptions for the shape of components are described as follows: (1) an arch ring section is an equal section, and any section is the design section size. (2) The assumption of pier column, tie beam, and so on section is that one side cannot be fitted effectively. If the corresponding parallel edge has been successfully fitted, then the translation strategy is adopted; otherwise, the design information is used for supplementation. (3) The T-beam section is consistent with the design size because the T-beam is modeled by aligning the design model with extract feature intersection points to the greatest extent using the ICP algorithm.

3.2. Data Segmentation. After pretreating the point clouds, the arch bridge point clouds are manually divided into four categories of components in Geomagic. The manual division time of the entire bridge is approximately 15 min. The first category is the arch ring. The second category is the pier column and tie beam. The third category is the pier, pier seat, and bent cap. The fourth category is the T-beam. The arch ring is the main stress structure of the arch bridge, as depicted by the rectangular stretching along the arch axis in Figure 2(a). The quality of several piers is crucial in identifying the stress of an arch bridge. The pier column and tie beam of the arch bridge are usually rectangular section components, as shown in Figure 2(b). The pier, pier seat, and bent cap of the arch bridge can be regarded as a standard contour along a line; hence, they are divided into the same category, as shown in Figure 2(c). The T-beam is the main component of the arch bridge deck, and it has a complex shape. However, in this study, the T-beam adopts the prefabrication method and has a unified size in the bridge, as shown in Figure 2(d).

3.3. Geometric Information Extraction

3.3.1. Arch Ring. As this study adopts the SSR method, the following two elements are required: (1) 2D cross section and (2) 3D path. For the arch ring, the complete point clouds of the arch-ring cross section are difficult to obtain. Changing the cross-sectional size of the arch ring has a negligible effect on the stress of the arch bridge. Thus, the design size of the 2D cross section is adopted. The 3D path of the arch ring is crucial in handling the stress of the arch bridge, further indicating that an accurate extraction algorithm is needed. First, a similar but nonidentical polynomial curve fitting method is used to describe the initial alignment of the arch ring [13]. Second, the obtained polynomial is used as the initial parameter of the sliding window algorithm to ensure an accurate extraction.

Polynomial curve fitting should meet two requirements to achieve the optimal results. First, the standard deviation between all points and each order of the polynomial curve fitting should be less than a given value (i.e., 0.5 m). Second, the standard deviation of the polynomial curve fitting should be less than that of a higher-order polynomial curve fitting. From the standard deviations of all points and each order of the polynomial curve fitting, the best polynomial curve fitting can then be selected. Figure 3 shows the solution process of the optimal polynomial curve fitting. The materials and methods section should contain sufficient detail so that all procedures can be repeated. It may be divided into headed subsections if several methods are described.

$$z = a_n . x^n + a_{n-1} . x^{n-1} + \ldots + a_2 . x^2 + a_1 . x^2 + a_0, \quad (1)$$

where x and z are the 2D coordinates of each point, and $a_0 - a_n$ represents the parameter to be estimated. The unknown parameters $a_0 - a_n$ are calculated using the least square method.

The specific steps of the sliding window algorithm are as follows: first, the best polynomial curve fitting is used to provide the slope of the tangent line at each interpolation point $\text{tangent}_j = f$. The normal direction is given by $\text{normal}_j = -1/\text{tangent}_j$. Then, the interval of the interpolation points is selected in accordance with the actual situation. Given the size of a long-span arch bridge, the interval is set to 1-2 m, as shown in Figure 4.

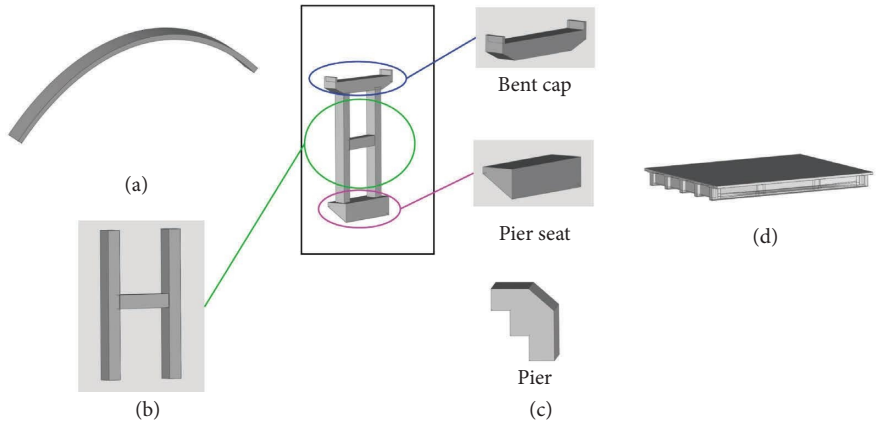

Figure 2: Illustrations of different components: (a) arch ring; (b) pier column and tie beam; (c) pier, pier seat, and bent cap; and (d) T-beam.

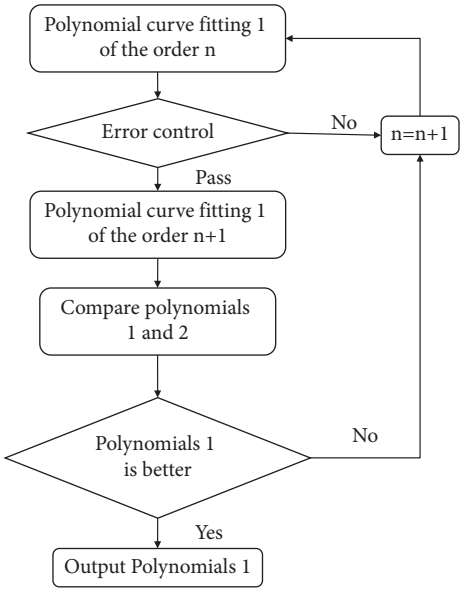

Figure 3: Process of the iterative polynomial fitting curve.

The rotation angle φ_j is derived from the angle between the normal direction of slice j and the global X-axis. In particular, the interpolation points of each slice j are used to calculate the normal direction of each slice. The changes in coordinates of the corresponding rotation angle $-\varphi_j$ for each window point cloud are determined as follows:

$$\begin{bmatrix} x' \\ y' \\ z' \end{bmatrix} = \begin{bmatrix} \cos\left(-\varphi_j\right) & \sin\left(-\varphi_j\right) & 0 \\ -\sin\left(-\varphi_j\right) & \cos\left(-\varphi_j\right) & 0 \\ 0 & 0 & 1 \end{bmatrix} \cdot \begin{bmatrix} x \\ y \\ z \end{bmatrix}. \quad (2)$$

The expected value of the window point cloud can then be solved. Finally, the expected value of each window point cloud is rotated such that it is given by $-\varphi_j$. The linear control points at the bottom of the arch ring can then be obtained. The cubic spline is used for the connection.

3.3.2. Pier Column and Tie Beam. The axis is the key geometric feature of the pier column and tie beam because these components are subjected to axial force. The perpendicularity of the pier column axis is taken as the key parameter in the detection. The pier column and tie beam of an arch bridge are usually rectangular. In view of ensuring the representativeness of our method, the rectangular cross-sectional pier column with two- and three-side point clouds is selected as the research object, as shown in Figure 5(a). The point clouds of the pier are segmented via the slicing method. The specific method involves cutting the data along the Z-axis in a plane parallel to the XY plane to obtain multiple cross sections, as shown in Figure 5(b). During site construction, the pier height of each pouring is 0.5–1 m. A 0.5–1 m length in the Z-direction is recommended. An improved RANSAC algorithm based on distribution density is adopted to extract the sections of the arch bridge components except the arch ring. For the sections that lack point

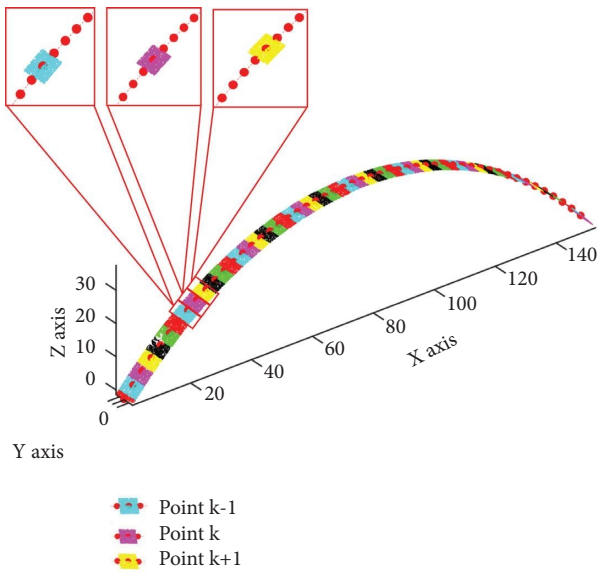

Figure 4: Slide window algorithm.

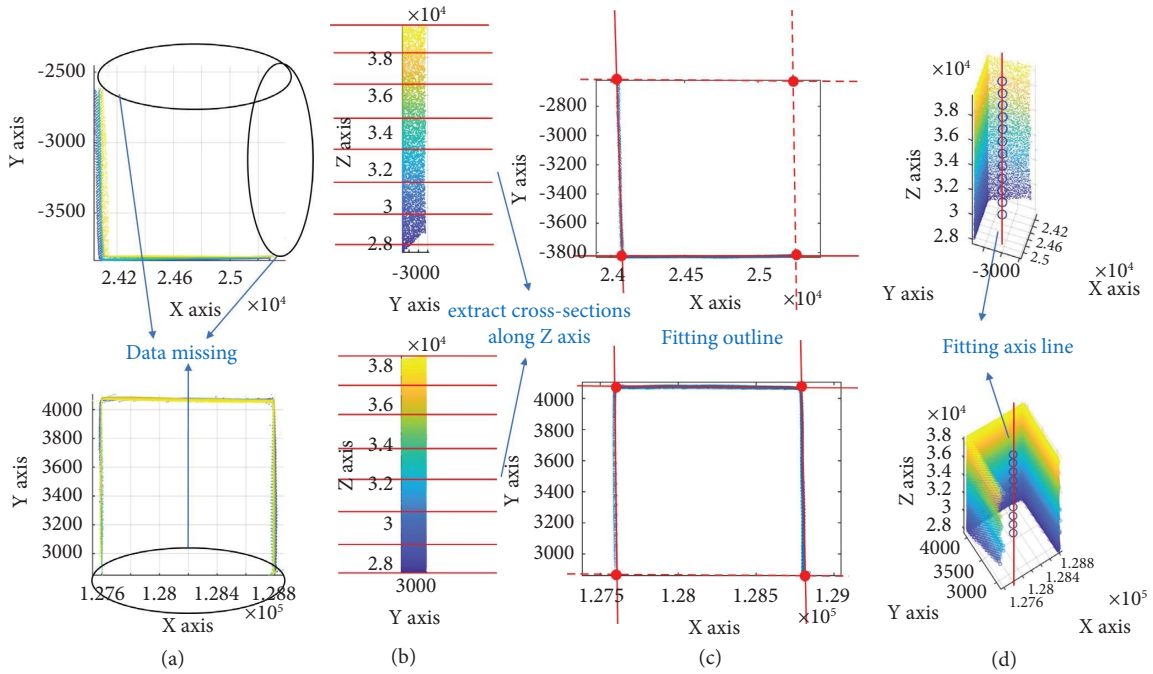

Figure 5: Illustrations of axis line for pier column and tie beam: (a) original point clouds, (b) extracted cross sections along the Z-axis, (c) fitting outline, and (d) fitting axis line.

clouds, the translation strategy is used to supplement the unknown line segment. Finally, the intersection of each line is obtained and then used to calculate the centroid of the intersection, as shown in Figure 5(c). The axis of the pier column is obtained via the least square method, as shown in Figure 5(d).

The specific steps of the improved RANSAC algorithm based on the distribution density algorithm are in the following steps, as shown in Figure 6. First, the number of point clouds per millimeter along the X-axis and Y-axis of each cross-section point clouds is calculated as m, and the average density is calculated as ρ. In addition, the density threshold is defined as ρ_t. Then, when $m \geq \rho_t$, the length T corresponding to the time point cloud is used as the threshold of the algorithm.

$$\rho_t = k\rho\,(k \in (3,5)), \tag{3}$$

where $\rho_x = N_a/a$, $\rho_y = N_b/b$; N_a and N_b represent the total number of points on the X-axis and Y-axis of the cross section, respectively; a and b represent the width and height

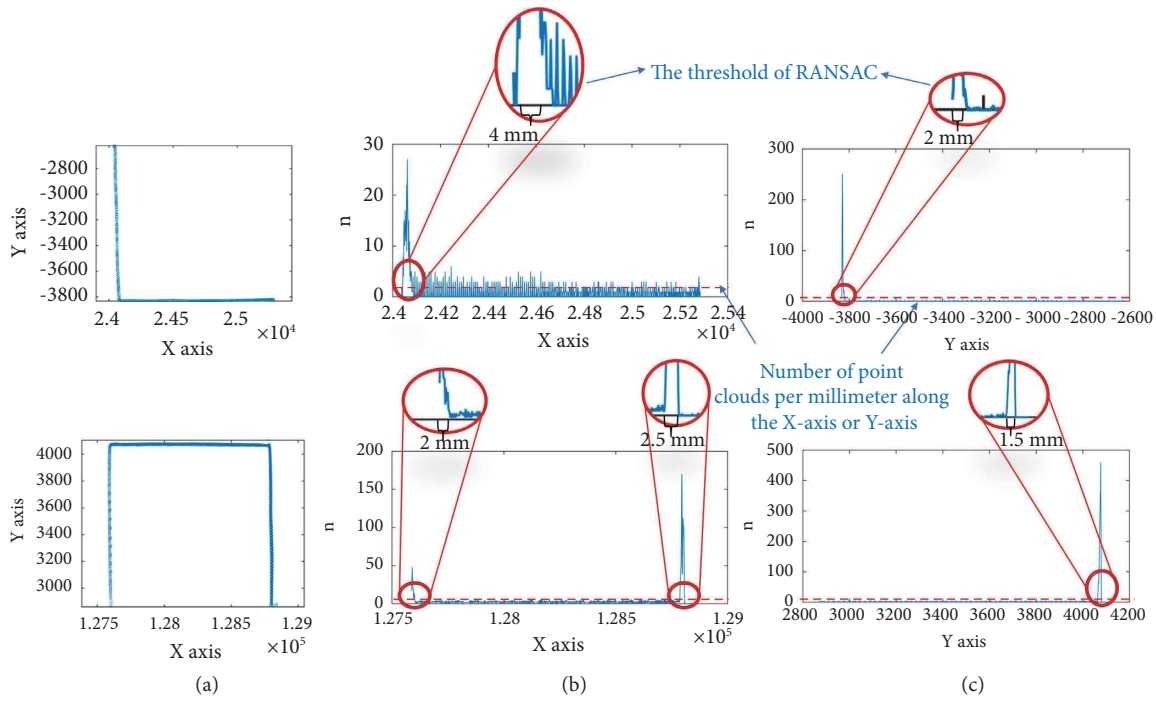

Figure 6: Calculation step of the threshold in RANSAC: (a) cross section of the point clouds, (b) number of point clouds per millimeter along X-axis, and (c) number of point clouds per millimeter along Y-axis.

Input: cross-sectional pier column with two-side point clouds list $Data_{n\times 3}$;
Output: The improved RANSAC algorithm's Distance threshold T, the axis of the pier column $\vec{l_0}$.
Dataz = Data$_{n\times 3}$ (:, 3);
$dz = 1000$; //Cut the interval of *Data* along the Z-axis in a plane parallel.
kz;//Quotient of total length of *Dataz* and *dz*.
$dx = 1$; //millimeter.
kx;//Number of millimeters along the X-axis of each cross section.
for $i = 1$to *kz* do
Datai; //Obtain the Point clouds of each segment of point clouds after cutting.
N_a, *a*;//N_a is the total number of points on the X-axis a of the cross section. *a* is the width of the cross section.
$\rho_x = N_a/a$; //The average density is calculated ρ Along the X axis.
$\rho_t = 3 * \rho_x$; //Definition the density threshold.
for $j = 1$to *kx* do
m_x; //Calculated the number of point clouds per millimeter along X-axis.
end for
Tx; //Find the number greater than ρ_t in m_x, and then the product of *dx*.
Ty; //It is the same as the solution process *Tx*.
l_1 = RANSAC (*Data*, *Tx*); //Using RANSAC algorithm to fit straight line.
Data0; //Delete the point cloud in Data used in l_1
l_2 = RANSAC (*Data*0, *Ty*); //Using RANSAC algorithm to fit remaining straight line.
$l_3 = l_1 + (0, 0, a)$; //the translation strategy is used to supplement the unknown line segment.
$l_4 = l_2 + (0, 0, b)$; //like l_3.
[P_{t1}, P_{t2}, P_{t3}, P_{t4}]; //calculate the intersection of l_1, l_2, l_3, l_4.
P_c; //calculate the centroid of the intersection.
end for
$\vec{l_0}$; //calculate the axis of the pier column.

Algorithm 1: Improved RANSAC algorithm.

of the cross section, respectively. The RANSAC algorithm of threshold T is used to fit the straight line of the cross section iteratively. The specific algorithm for calculating the axis of the pier column is given in Algorithm 1.

3.3.3. Pier, Pier Seat, and Bent Cap. The pier, pier seat, and bent cap of an arch bridge can be regarded as having a standard contour along one line; thus, they can be classified in the same category. These components are not necessarily perfectly vertical; however, the piers are assumed to be quasivertical in this study. First, the piers and pier seat are projected onto the XZ plane, as shown in Figures 7(a) and 7(b). The bent cap is projected onto the XY plane, as shown in Figure 7(c). The 2D ConcaveHull α-shape [22] is used to describe the outline of the slice cross section of the point clouds. Similarly, the improved RANSAC algorithm in Section 3.3.2 is adopted to extract the sections. In particular, their point clouds are absent because of the shielding of the soil around the pier and the diminutive size of the stops, which are similar to those of the pier column and tie beam, on both sides of the bent cap.

3.3.4. T-Beam. Most beam–slab bridges use precast concrete members as the main structural members [34]. The T-beam of an arch bridge is the same. The superstructure of arch bridges is the same as that of beam–slab bridges. Usually, the point clouds on both sides of the T-beam are difficult to determine, hence the incomplete data. Therefore, the point clouds of one side of the T-beam are selected in this research. The T-beam entails a complex modeling, further suggesting the inapplicability of the translation strategy.

The point clouds of the pier are segmented via the slicing method. In particular, the data along the X-axis in a plane parallel to the YZ plane are cut to obtain multiple cross sections, as shown in Figure 8 (a). A 0.5–1 mm length in the X-direction is recommended. The improved RANSAC algorithm based on distribution identity is used to obtain some characteristic intersections of the T-beams. And the calculated threshold of the improved RANSAC is shown in 8 (b). The characteristic intersections of each T-beam section total four, as shown in Figure 8 (c). The model alignment algorithm is proposed to best match the characteristic intersections extracted by the improved RANSAC algorithm and the points corresponding to the design model. For the T-beam, a model-aligning algorithm is proposed. In particular, the outline of some characteristic intersections of T-beams is obtained. Then, the iterative closest point (ICP) algorithm is used to match characteristic intersections and the points corresponding to the design model.

3.4. Bridge gDT Generation. After geometric information of the components is extracted as derived from the point clouds, it is stored in an Excel file. By automatically assigning the coordinates stored in Excel to the corresponding PART module of CATIA, the arch bridge gDT can also be established in CATIA. The three steps of this approach can be described as follows:

Step 1 : Generation of the arch bridge skeleton. Except for the T-beam characteristic intersections, the skeleton includes the 3D path and projection plane of the other components. First, the coordinate system of the entire arch bridge is determined through an approach that is essentially the same as that of the construction coordinate system. Then, the information is imported into CATIA's PART module, as shown in Figure 9(a).

Step 2 : Generation of the templates for each component. First, the local coordinate system is created in the PART module of CATIA. The Z-axis is in the 3D path, which is defined as a straight line or a curve. The X- and Y-axes should conform to the principles of the Cartesian coordinate system. Then, the origin of the component is determined. For the arch ring, pier, and tie beam, the origin is the center point of the profile. For the pier, pier seat, bent cap, and T-beam, the origin is the corner of the profile. Finally, the corners of the cross section are sketched and then connected with the segments, as shown in Figure 9(b).

Step 3 : Lofting of each component. The generation component templates are lofted on the arch bridge skeleton, as shown in Figure 9(c).

4. Experiments

4.1. Point Cloud Acquisition and Processing. The proposed semiautomatic method for extracting the geometric information of the bridge's components in the absence of point clouds was verified in this study. We used a Leica 3D laser scanner to collect the point clouds of a long-span arch bridge. The vertical and horizontal fields of view of the scanner were 300° and 360°, respectively. The distance between two points at a distance of 10 m in the resolution gear was approximately 3 mm, and the data collection time of each scan was approximately 13 minutes. Similar to the stations of cable-stayed and suspension bridges, the comprehensive data collection stations in this study were difficult to set up because of the model's large span, narrow site, and limited field of vision. In accordance with the actual situation of the bridge, three stations must be set up to obtain the required point clouds in Figure 10 (a). The point clouds of the three stations were registered using the ICP algorithm in CloudCompare software, as shown in Figure 10 (b). Among them, the first station was considered the target station. A total of 48,300 points in the joint station of the second and first stations were processed, and the final RMS was 0.0021 m. In addition, a total of 42,380 points in the third and first stations were processed, and the final RMS was 0.0018 m. To ensure the accuracy of

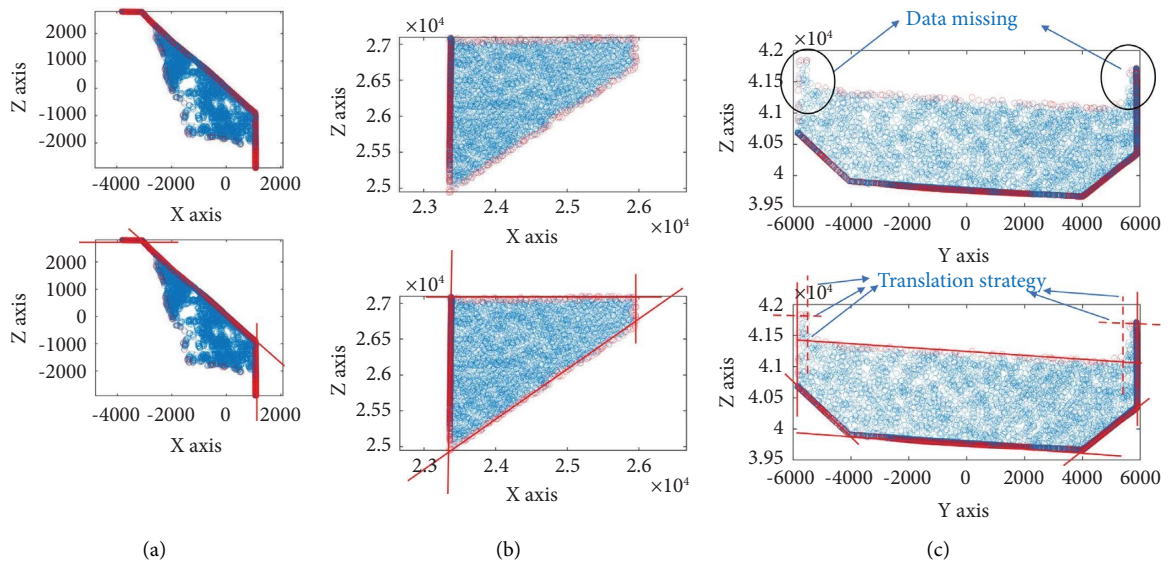

Figure 7: Illustrations of cross section: (a) pier, (b) pier seat, and (c) bent cap.

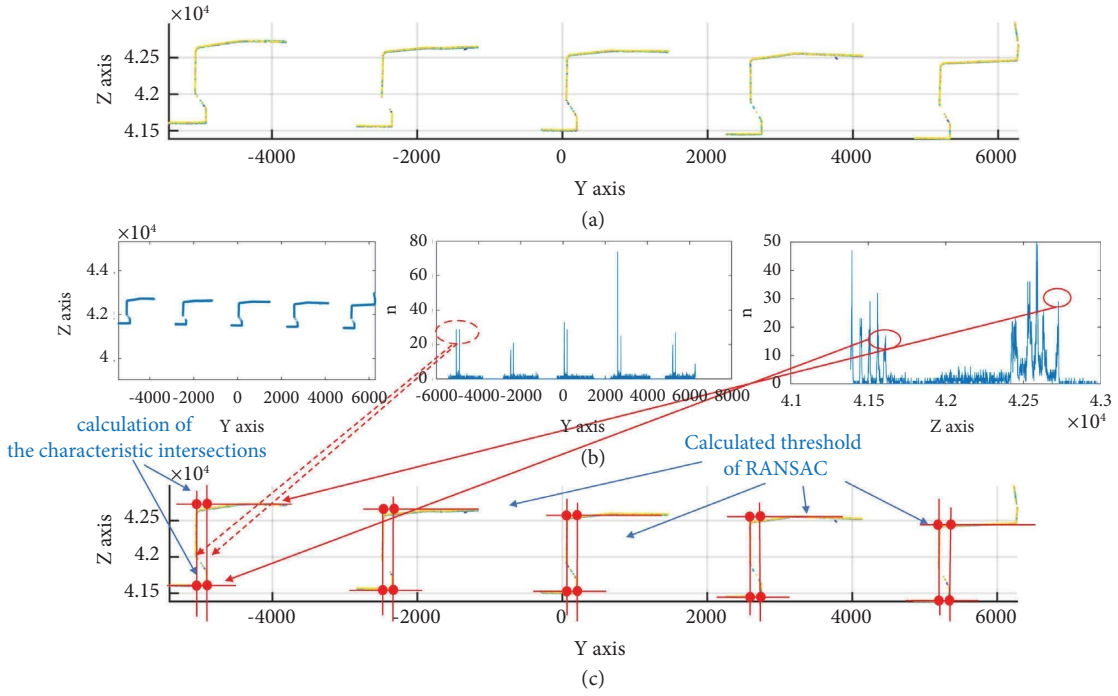

Figure 8: Illustrations of characteristic intersections for T-beam: (a) original point clouds, (b) calculated threshold of RANSAC, and (c) calculation of the characteristic intersections.

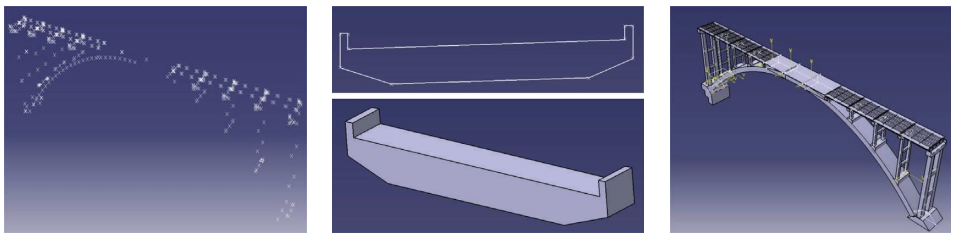

Figure 9: Illustration of gDT generation: (a) generation of the arch bridge skeleton, (b) generation templates for component, and (c) lofting of each component.

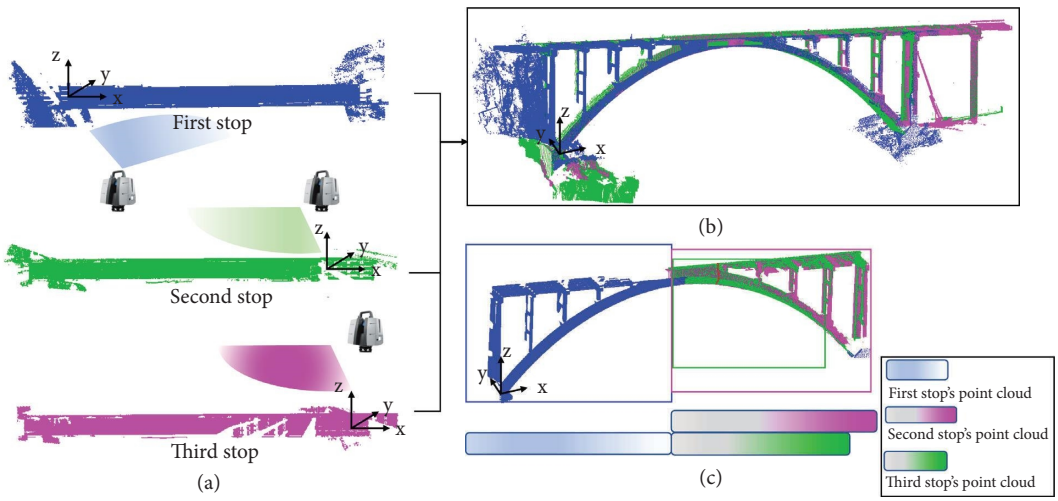

FIGURE 10: Illustration of gDT generation: (a) arch bridge scanning, (b) station processed by the ICP algorithm, and (c) point cloud used for generating gDT.

gDT generation, only about half of the point clouds in each station were selected in Figure 10 (c).

First, the Geomagic software is used for data segmentation and data format conversion. The bridge was composed of an arch ring, 16 pier columns, 12 tie beams, two piers, 16 pier seats, eight bent caps, and 10 span T-beams. These components were manually separated and saved as .txt files, including the X, Y, and Z coordinates of each point. Then, each txt file was imported into MATLAB to execute the algorithms developed for the different components. The creation sequence was in the order of arch ring, pier column, tie beam, pier, pier seat, bent cap, and T-beam.

4.2. Results. The method described in Section 3.4 was used to generate the gDT of the arch bridge. To check the original coordinate matching degree between the gDT and its point clouds, we converted the point clouds before segmentation and the reconstructed CATIA model into STP format and then imported them into Geomagic. We imported the bridge point clouds before segmentation, followed by the gDT of the arch bridge, into Geomagic. Figure 11 shows the coincidence of the two components and the deviation chromatogram of the arch ring, pier column, tie beam, pier, pier seat, bent cap, and T-beam. The deviation between the point clouds of some components and their gDT was evenly distributed, and most of them were within 5 mm.

Except for the absence point cloud, most other point clouds and their gDT coincide with each other, as illustrated in Figure 11. Some deviations can be observed in some parts of each component. This phenomenon can be attributed to three reasons: (1) the small amount of noise in the point clouds, (2) the format conversion between models in the software, and (3) the error of the cross-sectional fitting algorithm.

The arch ring linear is critical to the mechanical performance of the arch bridge. Taking the actual point cloud as a reference, the results of distance deviation between the polynomial curve fitting and the algorithm in this paper are compared. Among them, the root mean square error (RMSE) of the polynomial fitting curve algorithm is 0.0126 m, and the RMSE of the algorithm in this paper is 0.0055 m, which indicates that the latter is better in fitting the arch line. Among them, there are several obvious abnormalities in the distance deviation of the polynomial fitting curve algorithm, such as the midspan and quarter of the arch ring as depicted in Figure 12. The enlarged index of these corresponding positions shows that, compared with the control points of the algorithm in this paper are closer to the point cloud, the alignment of the polynomial fitting curve algorithm is farther from the point cloud, which further illustrates the progress of the algorithm in this paper.

In addition, the quality of the pier columns is important to the arch bridge. Here, the geometric information of the extracted pier column was compared with the design information in the construction drawing in two aspects: (1) intersection of the pier column centerline and pier base horizontal line and (2) perpendicularity. The results showed that the deviation of the intersection relative to the design intersection has a normal distribution. Moreover, the RMSE of the deviation was 0.0041 m, as depicted in Figure 13. The deviation between the perpendicularity of the pier column and the design angle in terms of RMSE was 0.046°, as shown in Figure 14. According to Klein et al. [35], an error of approximately 2% is acceptable in the as-built BIM model facility management.

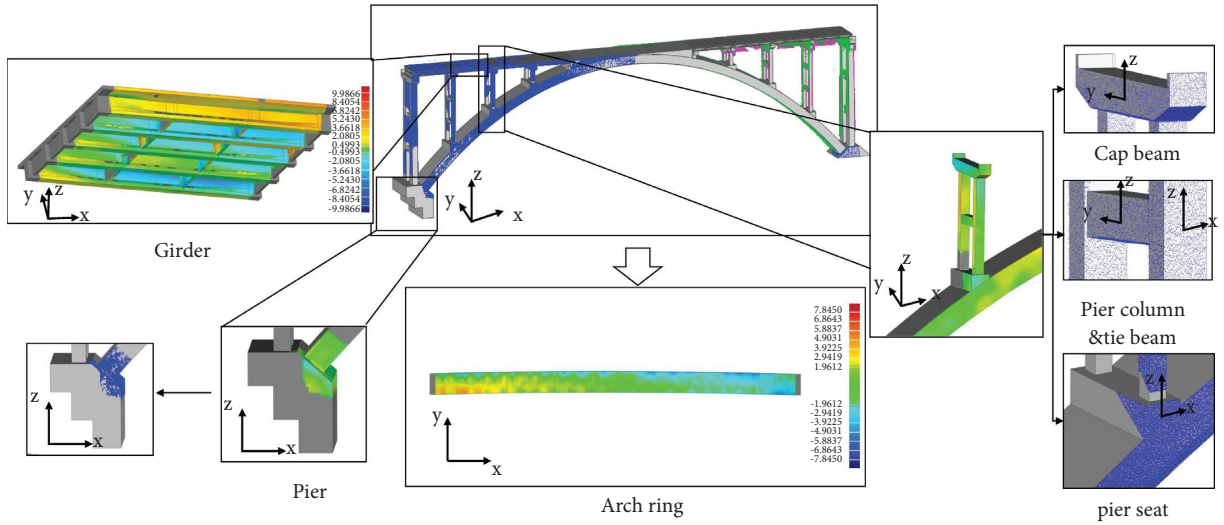

Figure 11: Deviation chromatogram of the arch bridge components, unit: mm.

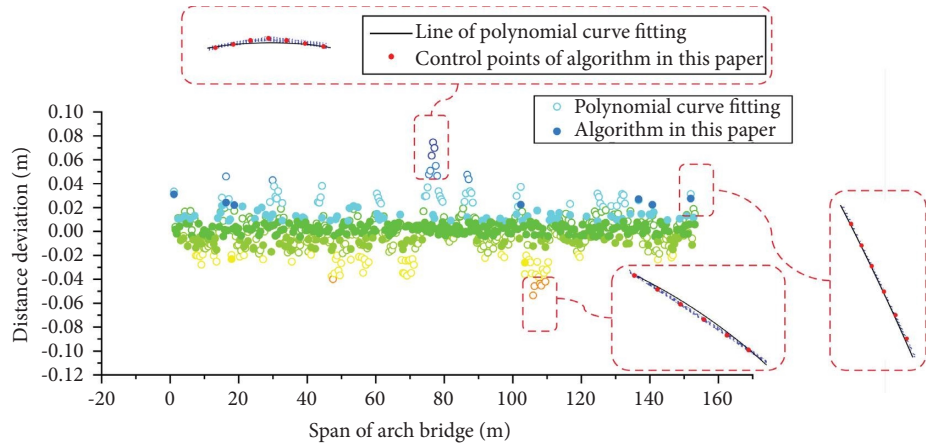

Figure 12: Accuracy analysis of arch ring linear algorithm.

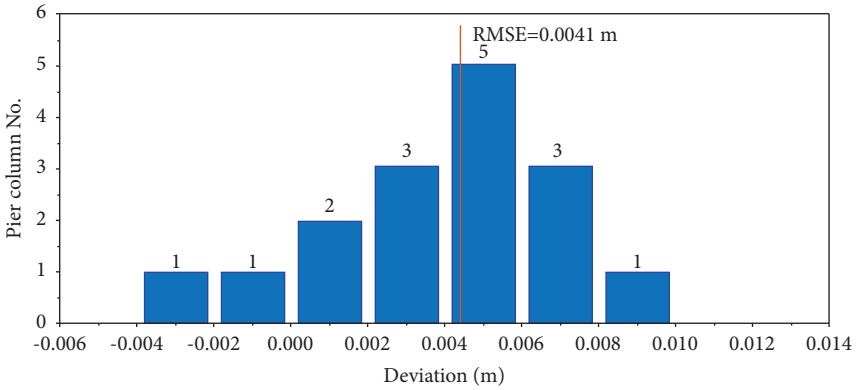

Figure 13: Deviation of the intersection relative to the design intersection.

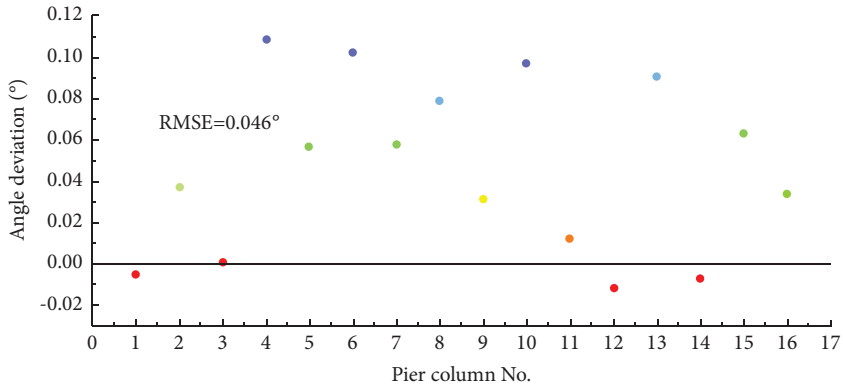

Figure 14: Deviation between the perpendicularity of the pier column and the design angle.

5. Conclusions and Prospect

This study proposed a semiautomatic method to extract geometric information of bridge components in the absence of point clouds. The arch bridge components included the arch ring, pier column, tie beam, pier, pier seat, bent cap, and T-beams. Geometric information was extracted from point clouds, and it included the following: arch ring alignment; centerline and contour of the pier column and tie beam; contour of the pier, pier seat, and bent cap; and feature points that match the T-beam. After the geometric information of each structural member from the point clouds was extracted, information was stored in an Excel file. The coordinates stored in Excel were automatically assigned to the corresponding module of CATIA, and the gDT of the arch bridge was generated in CATIA.

The method was verified on a large-arch bridge. During geometric information extraction, the arch ring, 16 pier columns, 12 tie beams, two piers, 16 pier seats, eight bent caps, and 10 prefabricated box girders of the arch bridge were successfully extracted. The deviation between the point cloud and the gDT model of the reconstructed bridge was distributed in Geomagic. The deviation chromatogram showed that the deviation between the point cloud of each component and the gDT model of the reconstructed bridge was evenly distributed, and most of them were within 5 mm. Subsequently, the geometric information of various pier columns was compared with the design information in the construction drawings in two aspects: (1) intersection of the pier column centerline and pier seat horizontal line and (2) perpendicularity. Results show that the deviation of the intersection relative to the design intersection entailed a normal distribution. Furthermore, the RMSE of the deviation was 0.0041 m. Results also indicate that our method can accurately extract the geometric features of arch bridge components from the point cloud data of arch bridges with defects.

Compared with traditional methods, the innovation in this study can be summarized as follows: first, the algorithm in this paper combines the advantages of the iterative polynomial algorithm and the sliding window algorithm, which can obtain a more accurate and stable fitting of the local alignment of the arch bridge compared with the traditional algorithm. Second, for the cross section of components with missing point clouds, the improved RANSAC algorithm uses a translation strategy to supplement unknown line segments to extract the characteristics of components. Third, researchers suggested using a template matching method to find the best match girder type in existing forecast bridge beam catalogues due to the complexity of the T-beam [15]. Three criteria for model matching include (1) span length, (2) girder bottom flange, and (3) web depth. The database is the standard product of the American Association of State Highway and Transportation Officials and the Bridge Beam Manual provided by BANAGHER Precast Concrete. However, a particularly accurate T-beam model may not be found due to the limitation of the database. The proposed algorithm in this paper can be applied to any T-beam to best match the design model and characteristic intersections.

Although this study shows promising results, certain limitations should be addressed. First, most of the cross-sectional forms of bridge members in this study were composed of multiple straight lines. Future research may extend the algorithm to other common types of member sections, such as the circular section and the section composed of multiple curve segments. Second, our method involved a manual segmentation process. Future studies may focus on local feature detection and other methods to segment various components automatically and improve the efficiency of data processing. Finally, gDT models should be able to handle additional mechanical information to realize the establishment of DTs further.

Data Availability

The data used to support the findings of this study are available from the corresponding author upon request.

Conflicts of Interest

The authors declare that there are no conflicts of interest regarding the publication of this paper.

References

[1] J. M. Andrić and D. G. Lu, "Risk assessment of bridges under multiple hazards in operation period," *Safety Science*, vol. 83, pp. 80–92, 2016.

[2] D. M. Baker and M. Cullimore, "Operation and maintenance of the clifton suspension bridge," *Europhysics News*, vol. 44, no. 2, pp. 16–20, 2015.

[3] A. Parrott and W. Lane, *Industry 4.0 and the Digital Twin*, Deloitte University Press, NY, US, 2017.

[4] R. Lopez and P. E. D. Love, "Design error costs in construction projects," *Journal of Construction Engineering and Management*, vol. 138, no. 5, pp. 585–593, 2012.

[5] D. Honfi, I. Bjornsson, O. L. Ivanov, and J. Leander, "Informed successive condition assessments in bridge maintenance," *Journal of Civil Structural Health Monitoring*, vol. 10, no. 4, pp. 729–737, 2020.

[6] V. Kankare, M. Holopainen, M. Vastaranta et al., "Individual tree biomass estimation using terrestrial laser scanning," *ISPRS Journal of Photogrammetry and Remote Sensing*, vol. 75, no. 1, pp. 64–75, 2013.

[7] M. Hochmuth, "Parameterized bridge design - conceptual, preliminary and detailed design," *Bautechnik*, vol. 93, no. 3, pp. 162–169, 2016.

[8] C. Wang, Y. K. Cho, and C. Kim, "Automatic BIM component extraction from point clouds of existing buildings for sustainability applications," *Automation in Construction*, vol. 93, no. 3, pp. 1–13, 2015.

[9] C. H. P. Nguyen and Y. Choi, "Comparison of point cloud data and 3D CAD data for on-site dimensional inspection of industrial plant piping systems," *Automation in Construction*, vol. 91, pp. 44–52, 2018.

[10] H. M. Lee and H. S. Park, "Gage-free stress estimation of a beam-like structure based on terrestrial laser scanning," *Computer-Aided Civil and Infrastructure Engineering*, vol. 26, no. 8, pp. 647–658, 2011.

[11] R. Lu and I. Brilakis, "Digital twinning of existing reinforced concrete bridges from labelled point clusters," *Automation in Construction*, vol. 105, pp. 102837–102837 16, 2019.

[12] G. Qin, Y. Zhou, K. Hu, D. Han, and C. Ying, "Automated reconstruction of parametric BIM for bridge based on terrestrial laser scanning data," *Advances in Civil Engineering*, vol. 2021, pp. 1–17, 2021.

[13] H. Yang, X. Y. Xu, and I. Neumann, "Deformation behavior analysis of composite structures under monotonic loads based on terrestrial laser scanning technology," *Composite Structures*, vol. 183, pp. 594–599, 2018.

[14] B. Riveiro, M. J. Dejong, and B. Conde, "Automated processing of large point clouds for structural health monitoring of masonry arch bridges," *Automation in Construction*, vol. 72, pp. 258–268, 2016.

[15] L. Yang, J. C. Cheng, and Q. Wang, "Semi-automated generation of parametric BIM for steel structures based on terrestrial laser scanning data," *Automation in Construction*, vol. 112, Article ID 103037, 2020.

[16] C. Thomson and J. Boehm, "Automatic geometry generation from point clouds for BIM," *Remote Sensing*, vol. 7, no. 9, pp. 11753–11775, 2015.

[17] W. F. Chen and L. Duan, *Bridge Engineering Handbook: Construction and Maintenance, Bridge Engineering*, Springer, Berlin, Germany, 2014.

[18] F. A. Limberger and M. M. Oliveira, "Real-time detection of planar regions in unorganized point clouds," *Pattern Recognition*, vol. 48, no. 6, pp. 2043–2053, 2015.

[19] R. Schnabel, R. Wahl, and R. Klein, "Efficient RANSAC for point-cloud shape detection," *Computer Graphics Forum*, vol. 26, no. 2, pp. 214–226, 2007.

[20] J. Chen, C. Zhang, and P. Tang, "Geometry-based optimized point cloud compression methodology for construction and infrastructure management," in *Proceedings of the ASCE International Workshop on Computing in Civil Engineering*, pp. 377–385, IEEE, Seattle, WA, USA, June 2017.

[21] R. Ramamurth, K. Harding, and X. Du, "Geometric and topological feature extraction of linear segments from 2D cross-section data of 3D point clouds," *SPIE Sensing Technology Applications*, vol. 9489, pp. 236–247, 2015.

[22] A. J. C. Moreira and M. Y. Santos, "Concave hull: a k-nearest neighbours approach for the computation of the region occupied by a set of points," in *Proceedings of the GRAPP 2007 Second International Conference on Computer Graphics Theory and Applications GM/R. DBLP*, IEEE, Barcelona, Spain, March 2007.

[23] D. F. Laefer and L. Truong-Hong, "Toward automatic generation of 3D steel structures for building information modelling," *Automation in Construction*, vol. 74, pp. 66–77, 2017.

[24] Y. Zhou, D. Han, K. Hu et al., "Accurate virtual trial assembly method of prefabricated steel components using terrestrial laser scanning," *Advances in Civil Engineering*, vol. 2021, no. 15, pp. 1–15, 2021.

[25] U. Bauer and K. Polthier, "Generating parametric models of tubes from laser scans," *Computer-Aided Design*, vol. 41, no. 10, pp. 719–729, 2009.

[26] J. Jung, C. Stachniss, S. Ju, and J. Heo, "Automated 3D volumetric reconstruction of multiple-room building interiors for as-built bim," *Advanced Engineering Informatics*, vol. 38, no. 10, pp. 811–825, 2018.

[27] T. K. Danielle, E. N. Tchinda, and C. Bobda, "From PC2BIM: automatic model generation from indoor point cloud," in *Proceedings of the 13th International Conference on Distributed Smart Cameras*, vol. 23, IEEE, New York, NY, USA, September 2019.

[28] L. Barazzetti, F. Banfi, and R. Brumana, "BIM from Laser Clouds and Finite Element Analysis: Combining Structural Analysis and Geometric Complexity," *International Archives of the Photogrammetry Remote Sensing and Spatial Information Sciences*, vol. 40, pp. 345–350, 2015.

[29] R. Quattrini, E. S. Malinverni, P. Clini, R. Nespeca, and E. Orlietti, "From TLS to HBIM: high quality semantically-aware 3D modeling of complex architecture," *The International Archives of the Photogrammetry, Remote Sensing and Spatial Information Sciences*, pp. 367–374, 2015.

[30] P. Tang, D. Huber, B. Akinci, R. Lipman, and A. Lytle, "Automatic reconstruction of as-built building information models from laser-scanned point clouds: a review of related techniques," *Automation in Construction*, vol. 19, no. 7, pp. 829–843, 2010.

[31] E. Agapaki and I. Brilakis, "State-of-Practice on As-Is Modelling of Industrial Facilities S," *Advanced Computing Strategies for Engineering*, pp. 103–124, 2018.

[32] H. Son, F. Bosche, and C. Kim, "As-built data acquisition and its use in production monitoring and automated layout of civil infrastructure: a survey," *Advanced Engineering Informatics*, vol. 29, no. 2, pp. 172–183, 2015.

[33] E. Hoffman, "Specifying laser scanning services," *Chemical Engineering Progress*, vol. 101, no. 5, pp. 34–38, 2005.

[34] M. K. Kim, S. McGovern, M. Belsky, C. Middleton, and I. Brilakis, "A suitability analysis of precast components for standardized bridge construction in the United Kingdom," *Procedia Engineering*, vol. 164, pp. 188–195, 2016.

[35] L. Klein, N. Li, and B. Becerik-Gerber, "Imaged-based verification of as-built documentation of operational buildings," *Automation in Construction*, vol. 21, pp. 161–171, 2012.